Ocean Systems Engineering, *Vol. 15, No. 4 (2025) 361-386*
https://doi.org/10.12989/ose.2025.15.4.361

An investigation of scale effects on towed cable system

Wang Zhibo* and Huan Shuaiyu[a]

School of ocean engineering, Jiangsu Ocean University, Lianyungang, Jiangsu, 222005, China

(Received September 23, 2024, Revised August 4, 2025, Accepted September 2, 2025)

Abstract. A one-way Fluid and Structure interaction method is introduced based on a lumped parameters method and a Reynolds-averaged Navier-Stokes solver with automatic viscous mesh generation. The lumped parameters method is numerically solved by fourth-order Runge-Kutta method. Unidirectional coupling by hydrodynamic interpolation and transformation from flow field to cable dynamics. A dimensional analysis is applied in this high Fluid and Structure Interaction (FSI) system. The Reynolds effects and Strouhal effects are both fully discussed. A two scale ratios model is applied in scale effect analysis. We found a similarity of hydrodynamic distribution and vortex shedding in scaled cable wake under only given two-ratios. The upper bound Reynolds effect is also discussed.

Keywords: fluid structure interaction; lumped mass method; reynolds number; scale effect; strouhal number; towed cable system

1. Introduction

There is a significant hydrodynamic interaction in a towed cable system. Especially in a deep-sea towed operation, the length of towed cable can extend to several kilometers from winch, posing significant challenges for precision simulation of flow pattern around cable. It often fails to provide accuracy simulation of diving depth and vibration on these hydrodynamic decided cable shapes.

The dynamic load distribution along cable has an unsatisfactory simulation from a scale model in laboratory. It is inaccurately extrapolated the results obtained from a scaled model to full-scale prototypes. This presents notable scale effects due to discrepancies in a multi-scale flow field around cable.

Reynolds number criterion is considered as the important guide for scaled model test in a towed cable hydrodynamic and many other underwater vehicles. Sezen *et al.* (2021) investigated scale effects on the benchmark DARPA SUBOFF submarine hull form's resistance, nominal wake and self-propulsion characteristics, including a representative full-scale submarine based on the DARPA SUBOFF. Farkas *et al*. (2018) found five extrapolation methods to extrapolate results from an extensive towing tank experiments to full-scale values. Pazwash and Robertson (1975), Zakeri *et al*. (2008), Wang *et al*. (2018), Haza *et al*. (2013) and Perez (2012) have made a series of down-scaled physical hydraulic model tests based on the principle of non-Newtonian fluid

*Corresponding author, Professor, E-mail: 2021000063@jou.edu.cn
[a] Ph.D., E-mail: 2022220308@jou.edu.cn

http://www.techno-press.org/?journal=ose&subpage=7 ISSN: 2093-6702 (Print), 2093-677X (Online)

dynamics. Terziev *et al*. (2019) have examined the scale effect on the resistance components for the benchmark Kriso Container Ship (KCS) using three scaled model. Dogrul *et al*. (2020) studied the scale effects on KCS hull form resistance components. The extrapolated results were compared with the full-scale numerical results, and the different decomposition methods were fully discussed. It was found that the Froude and Hughes extrapolation methods presented different results for the ships which have different block coefficients. Delen and Bal (2019) focused on the scale effects using Telfer geosim method for three different KCS models. The authors revised the original Telfer geosim formulation. The full-scale numerical results were compared with those of the model scales' extrapolated results using both the ITTC extrapolation method and revised Telfer geosim method. The comparisons showed that the revised method presented better results than the conventional ITTC extrapolation method.

Christian (2021) investigates the hydrodynamic scaling effects for a heave buoy Wavestar. Wang *et al*. (2016) used pod resistance influence factor to represent the effect of wake field of CRP on the pod resistance and a method of estimating the hydrodynamic performance was proposed for full scale propulsion system. Sun *et al*. (2020) analyzed the effects of the scale on evolution of propeller wake under open water conditions and pointed out that the kinetic energy of full-scale propellers is generally proportionally larger than that of model-scale propellers. Dong *et al*. (2018) compared the scale effects predicted by Reynolds-averaged Navier-Stokes (RANS) with those by the ITTC-1978 method. Li *et al*. (2020) developed a scaled model test system with a container stack and twist lock based on Buckingham's Theorem and the Froude scaling laws. Stanier (1998), Sanchez (2003), Li (2006), Muller *et al*. (2009), and Krasilnikov *et al*. (2009) have analyzed the scale effect of propellers' hydrodynamic performance using the RANS method, and found that the viscous force is dependent on Reynolds number.

Ji *et al*. (2021) have given a dimensionless coefficient to convert the model pump thrust into actual pump. Xie *et al*. (2021) investigated the scale effect of bow wave breaking for the standard ship model KCS. Wang and Wang (2019) investigated change regularity of load difference between inside and outside propeller under different scale ratios. Zhou [*et al*. (2020) judged similarity conditions of flow by researching on several typical flow phenomena and a new similarity theory is established.

According to towed system design survey, the diameter range of a commonly used towing cable is most between 1 cm and 18 cm in a winch selection or new design. Ocean towing speed are often in a range of 2knot and 20knot. These tow parameters result in a narrow range of Reynolds number less than 2×10^6 by considering cable diameters. The low Reynolds number flow around cable is a low frequency broadband excitation. In order to approach seabed more closely, towed device is designed to get a detailed scanning map. A precisely dynamic FSI model is developed to be the initial guidance of approaching observation.

This study investigates scale effects in a towed cable system simulation model and propose a novel fluid structure interaction system two-scaled ratio calculation procedure for towed cable system. lumped mass method is coupled with a (RANS) tool. An interpolation algorithm is also designed for drag force between scaled cable and full-scale cable. It is ensured a flow similarity based on geometric similarity, motion similarity, and dynamic similarity in FSI simulation system. Thus, the simulation of the prototype's authentic physical state is enabled by scale cable.

2. Computational methods

2.1 Model scale strategy

A full-scale deep sea towed cable system has a cable length over hundreds of meters in ocean trails. A simulation of flow around a full-scale towed system leads an unbearable high computational cost. The computational cost is enormous and difficult to achieve. For a length of 1000 m towed cable, the grid often involves several tens of millions in a RANS simulation. Rules in fluid-structure similarity have been widely applied, such as Oshiro *et al.* (2017), Neubeger *et al.* (2007). As described by Wu (2016) it is necessary to achieve mechanical similarity between the scale model and prototype in a fluid. It requires sanctification the conditions of geometric similarity, motion similarity, and dynamic similarity. Geometric similarity refers to the proportional scaling of all geometric dimensions and identical shapes between scaled-down model and prototype. Essentially, it requires of flow fields around a scaled cable similar to those of prototype's flow field. Cable is reduced to a fine thread of filament. This scaled model draws a significant difference of flow pattern with prototype.

In this study, geometric similarity is ensured by using scaled down nodal coordinates of towed cable profile. Motion similarity refers to the similarity of velocity and acceleration of flow fields between scaled-down model and prototype. It demands all corresponding spatial proportional relationship in the flow fields of scaled-down model and prototype. Both have the same direction of velocity and acceleration at corresponding locations and the magnitudes of velocity are also proportional.

Dynamic similarity refers to a ratio of dynamic field between scaled-down cable and prototype. Specifically, it requires that all corresponding pressure and velocity on cable in the flow fields of scaled-down model and prototype both have the same distribution. The magnitudes of hydrodynamics are also proportional.

For viscous flows, Re is a significant similarity parameter, and to achieve similarity in unsteady flows, S_t should be kept constant for scaled model. Fr represents the gravity similarity condition between scaled-down model and prototype, which is relevant to free surface wave generation on the water surface. However, since towed cable system typically operate at greater depths below the water surface, the consideration of Fr can be omitted.

2.2 Cable dynamics system

Similar to cable dynamic framework built by Wang *et al.* (2019). A global coordinate system and a local coordinate system are established to describe the motion of towed cable system. The global coordinate system takes the surface end of towed cable as coordinate origin, with mother ship tow maneuver located in the XOY plane. The -Z direction corresponds to water depth, and towing direction along +X-axis. The element position is described by nodal coordinates (X, Y, Z). The local coordinate system is used (x, y, z) to describe element position, where the x-axis along cable axis, and y and z perpendicular to the x-axis. The transformation relationship between the two coordinate systems is given by Eq. (1).

$$\begin{bmatrix} X \\ Y \\ Z \end{bmatrix} = Q \begin{bmatrix} x \\ y \\ z \end{bmatrix} \tag{1}$$

where Q is coordinate transformation matrix between local and global coordinate system.

$$Q = \begin{bmatrix} cos\theta_x cos\theta_y cos\theta_z & 0 & 0 & 0 \\ 0 & 0 & 0 & 0 & 0 & 0 \\ 0 & 0 & 0 & 0 & 0 & 0 \\ 0 & 0 & 0 & cos\theta_x cos\theta_y cos\theta_z \\ 0 & 0 & 0 & 0 & 0 & 0 \\ 0 & 0 & 0 & 0 & 0 & 0 \end{bmatrix}$$

The governing equation for a cable element in the towed cable is given by Eq. (2)

$$M\ddot{x} = \frac{\partial T}{\partial s} + B + G + D \tag{2}$$

where M is the mass matrix of cable element, T is the inertial forces, D represents the drag forces, G is gravity force, B is buoyancy and x is node position vector.

Following the principle of lumped mass method, the towed cable is discretized into N segments, comprising N+1 nodes, where the tail end corresponds to the i=0-th node, and the upper end corresponds to the *i*=N-th node.

Applying Newton's second law to the *i*-th node yields the fundamental governing equation for the cable element as in Eq. (3).

$$M_i\ddot{x}_i = F_i = \Delta T_i + B_i + G_i + D_i \tag{3}$$

where M_i is the mass matrix, includes the cable element's inertial mass and its added mass in the water. $\ddot{x}_i$ is acceleration. F_i is all external forces acting on the i-th cable element, includes the inertial forces in towed cable ΔT_i, buoyancy B_i, gravity G_i, and drag force D_i. These parameters are solved by central scheme, and their calculation formulas are given as follows.

The inertial forces are generated due to the elastic properties of towed cable and acts in the tangential direction. Assuming small strains, the linear stress-strain relationship can be utilized to obtain relations as Eq. (4).

$$\begin{cases} \Delta T_i = T_{i+1/2} - T_{i-1/2} \\ T_{i+1/2} = E\sigma\varepsilon_{i+1/2}\tau_{i+1/2} \\ \varepsilon_{i+1/2} = \frac{|x_{i+1} - x_i|}{l_{i+\frac{1}{2}}} - 1 \end{cases} \tag{4}$$

where τ is the unit tangential vector of towed cable, which can be obtained by differentiating positional vector with respect to arc length. E represents effective elastic modulus, and x_i is a position vector of node i in global coordinate system. A similar form can be derived for inertial forces $T_{i-1/2}$.

The forces resulting from buoyancy and gravity are given by Eq. (5).

$$B_i + G_i = -0.5\rho\left(l_{i-\frac{1}{2}}\sigma_{i-\frac{1}{2}} + l_{i+\frac{1}{2}}\sigma_{i+\frac{1}{2}}\right)g + 0.5(\mu_{i-\frac{1}{2}}l_{i-\frac{1}{2}} + \mu_{i+1/2}l_{i+1/2})g \tag{5}$$

where g is acceleration due to gravity.

Drag arises from relative motion between towed cable and surrounded fluid. Under this assumption, it can be decomposed into normal and tangential component, each component is function of a relative velocity. It can be expressed in Eq. (6).

$$D_i = 0.5\left(D_{i-\frac{1}{2}} + D_{i+\frac{1}{2}}\right) \tag{6}$$

where $D_{i-\frac{1}{2}} = C_{\left(i-\frac{1}{2}\right)x}\left(\frac{1}{2}\rho V_{i-\frac{1}{2}}^2 ld\right)$, $D_{i+\frac{1}{2}} = C_{\left(i+\frac{1}{2}\right)x}(\frac{1}{2}\rho V_{i+1/2}^2 ld)$ both represent the hydrodynamics from CFD simulations.

The motion control equations for each towing cable can be derived from Eq. (7).

$$\begin{cases} \frac{d\dot{x}_i}{dt'} = M_i^{-1}F_i \\ \frac{dx_i}{dt'} = \dot{x}_i \end{cases} \tag{7}$$

Finally, the fourth-order Runge-Kutta method is employed to numerically integrate Eq. (7) in time domain.

2.3 Computational fluid dynamics model and data exchange

Flow field simulation should be able to accurately and efficiently simulate a separated boundary flow around towed cable. A cable is considered as a circular cross-section cable with smoothed surface. Within the commonly used towing speed range, there is a large scale of separate vortex in flow field. According to Wang and Wang (2019), the Reynolds-averaged Navier-Stokes (RANS) method is adopted, and the SST k-ω model is chosen to simulate the fluid flow around towed cable. The governing flow equations are as follows.

$$\frac{\partial(\rho k)}{\partial t} + \frac{\partial(\rho k u_i)}{\partial x_i} = \frac{\partial(\Gamma_k \frac{\partial k}{\partial x_j})}{\partial x_j} + G_k - Y_k + S_k \tag{8}$$

$$\frac{\partial(\rho \omega)}{\partial t} + \frac{\partial(\rho \omega u_i)}{\partial x_i} = \frac{\partial(\Gamma_\omega \frac{\partial \omega}{\partial x_j})}{\partial x_j} + G_\omega - Y_\omega + D_\omega + S_\omega \tag{9}$$

where G_k represents the turbulence kinetic energy, G_ω is the ω equation, Γ_k, Γ_ω are the effective diffusion terms for k and ω, respectively, Y_k, Y_ω are divergence terms for k and ω, and D_ω is orthogonal divergence term.

During the transfer of hydrodynamic in segments, the hydrodynamic components of D_j (F_{jx}, F_{jy}, F_{jz}) at each segment of a cable profile is given in Eq. (10) based on number of surface elements M.

$$F_{ix} = \sum_{j=1}^{M} p_{jx} + \tau_{jx}, F_{iy} = \sum_{j=1}^{M} p_{jy} + \tau_{jy}, F_{iz} = \sum_{j=1}^{M} p_{jz} + \tau_{jz} \tag{10}$$

If a normal CFD scaled model is adopted in this procedure, the non-dimensional coefficients are given as Eq. (11) and

$$C_{ix} = F_{ix}/(\tfrac{1}{2}\rho V_i^2 ld),\ C_{iy} = F_{iy}/(\tfrac{1}{2}\rho V_i^2 ld),\quad C_{iz} = F_{iz}/(\tfrac{1}{2}\rho V_i^2 ld) \tag{11}$$

The D_i in Eq. (6) is obtained by two adjacent segments as shown in Eq. (12) and Fig. 1 on condition of unscaled models.

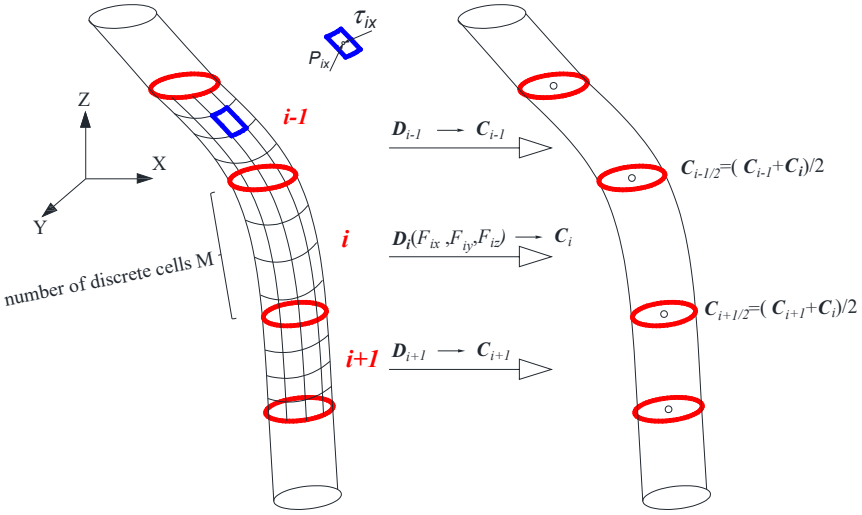

Fig. 1 One-way hydrodynamic transfer in segments

$$\begin{cases} C_{\left(i-\frac{1}{2}\right)x} = (C_{(i-1)x} + C_{(i+1)x})/2, \\ C_{\left(i-\frac{1}{2}\right)y} = (C_{(i-1)y} + C_{(i+1)y})/2, \\ C_{\left(i-\frac{1}{2}\right)z} = (C_{(i-1)z} + C_{(i+1)z})/2 \end{cases} \tag{12}$$

The transmission process is shown in the Fig. 1.

2.4 Fluid-structure interaction scheme design

An initial cable profile of towed cable is obtained by lumped mass method and experimentally validated, and the obtained cable nodal coordinates are scaled down according to given geometric scale ratio. A Computational Fluid Dynamic (CFD) topological multi-block structural mesh of flow field around this profile minification is programmatically generated by Gmsh and Remacle (2009) Hydrodynamic coefficients acting on the scaled cable are obtained by a CFD solver Fluent. Subsequently, hydrodynamic coefficients from CFD model are transformed into full scale cable profile in normalization by a load interpolation transformation polynomial in each model segment. The cable segments split is decided by inclinations of cable profile relative to towed directions. In a slow change of inclination, the length of segment is large and vice versa. In order to reach fluid-structure interaction (FSI) convergence, an iterative scheme is designed for stress deformation of flexible cable by traction and hydrodynamic load from scaled cable CFD model. This iterative scheme has a high efficiency in practices. Data processing between multi-scaled computational physical fields in Fig. 2 is decided by a cable profile convergence criterion. This FSI design is a one-way fluid-structure interaction, a possible high frequency vibration acted on flow and its reaction formation is neglected.

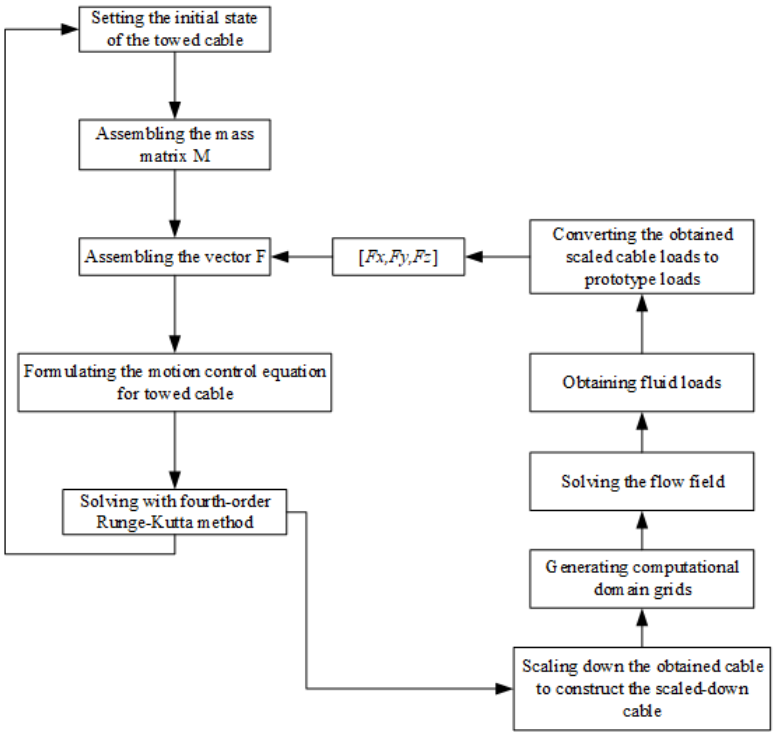

Fig. 2 Data flow and iterative diagram of fluid-structure interaction

The scale effect is explicitly driven by this FSI scheme. This FSI transformation is used to verify amplification or elimination of scale-dependent coupled system in this scaled CFD model with a full scale dynamic structural model. In this FSI treatment, there are two methods to deal with hydrodynamics transfer. One is a time averaged drag coefficients to a quasi-steady-state tow. The other is a transient transfer of drag coefficients to a dynamic tow.

3 Numerical modelling

3.1 CFD structured mesh and boundary conditions

Implementation of a high-accuracy structural mesh can be considered one of the difficulties in a CFD solution of flow field around a great slenderness of cable.

A geometric block C-H design is developed for mesh generation around towed cable tow by scripts in Gmsh and Remacle (2009), The computational domain was created around cable as shown in Fig. 3. The cross-sectional topology of computational domain is used as a source plane as in Fig. 4 for sweep. A three-dimensional mesh is generated by stretching this source topology region along a cable profile curve. Eqs. (13) and (14) are used for modeling turbulent boundary layer mesh refinement in CFD depended on implemented wall functions. The grid point distance of first layer near cable wall boundary is decided by dimensionless value y+ by Eqs. (13) and (14).

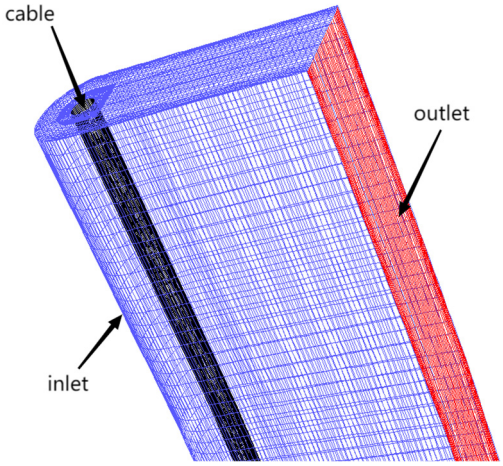

Fig. 3 Domain design and boundary

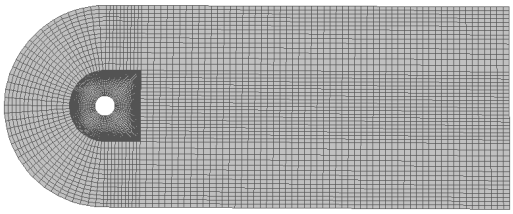

Fig. 4 Design of C-H type source topology

$$d_s = R\sqrt{80}y^+Re^{-13/14} \tag{13}$$

$$d_{s2} = 2d_s \tag{14}$$

3.2 Verification of scaled computation model

According to flow field similitude criteria, it is ensured that cable length Reynolds number in Eq. (15) is equal between scaled-down cable and its prototype. L_0 represents the length of prototype cable, L_1 is the length of scaled-down cable, and ν represents the kinematic viscosity.

$$R_{eL} = \frac{V_0 L_0}{\nu} = \frac{V_1 L_1}{\nu}$$

$$R_{eD} = \frac{V_0 D_0}{\nu} = \frac{V_1 D_1}{\nu} \tag{15}$$

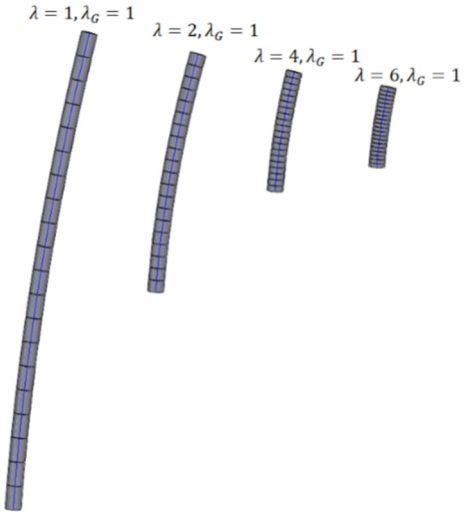

Fig. 5 Cable configurations in different tow-scaled ratio model

Table 1 Case with different cable shape scale ratios

cable scale ratios (λ)	towed speed(m/s)	cable length(m)	cable diameter scale ratios (λ_G)
6	$V_1 = V_0 \times 6$	$L_1 = L_0/6$	1
4	$V_1 = V_0 \times 4$	$L_1 = L_0/4$	1
2	$V_1 = V_0 \times 2$	$L_1 = L_0/2$	1

It can be obtained that $V_0L_0 = V_1L_1$, when $L_0 = \lambda L_1$. λ is the scaled-down ratio of cable profile in Eq. (13) and $V_1 = \lambda V_0$. However, it can be anticipated that the diameter $D_1 = \lambda D_0$ of cable is also becoming a miniature similar to thin filament with significant scale effects in a cylinder wake at such flow velocity V_1. We respectively introduce another cable diameter scale ratio to characterize the scaling of towed cable diameter. λ_G is the scaled-down ratio of cable diameter in Eq. (16). It is used to eliminate this cylinder flow scale effect. The cable configuration is given in Fig. 4

$$D_1 = D_0/\lambda_G \tag{16}$$

In general, ocean tow investigation is carried out with a towed speed no more than 20 m/s in most tow cases. The cable profile also has a large scale due to this speed limit. A set of scale ratios is designed to consider this coupled effect for the combination of λ and λ_G.

This relation of two scale ratios is presented in Table 1 and Fig. 5 with an invariant of cable diameter $\lambda_G = 1$, to maintain homogeneity in a cylinder's wake.

A towing tank experiment of full-scale towed cable system with 3 m cable length were adopted for validation from Guan *et al.* (2011) as shown in Table 2. This flexible cable is assumed a slender circular cross section. The structural torsion and bending are not considered in towed dynamic

Table 2 Parameters of towed system

Physical parameters of towed cable		Physical parameters of towed body	
Length	L=3 m	Mass	m=1 kg
Diameter	D=0.01 m	Drainage volume of towed body	0.00015 m3
Density	ρ=1050 kg/m3	Drag coefficient	C_{dx}=1.05, C_{dy}=0, C_{dz}=0.1
Weight of per unit length	μ=0.082 kg/m	Buoyancy	1.47 N
Bending stiffness	0 kN·m2	Towed speeds V0	0.3 m/s
Poisson ratio	0.28		
Axial stiffness	110kN		
Torsional stiffness	0 kN·m2		
Initial Cn	1.2		
Initial Ct	0.025		

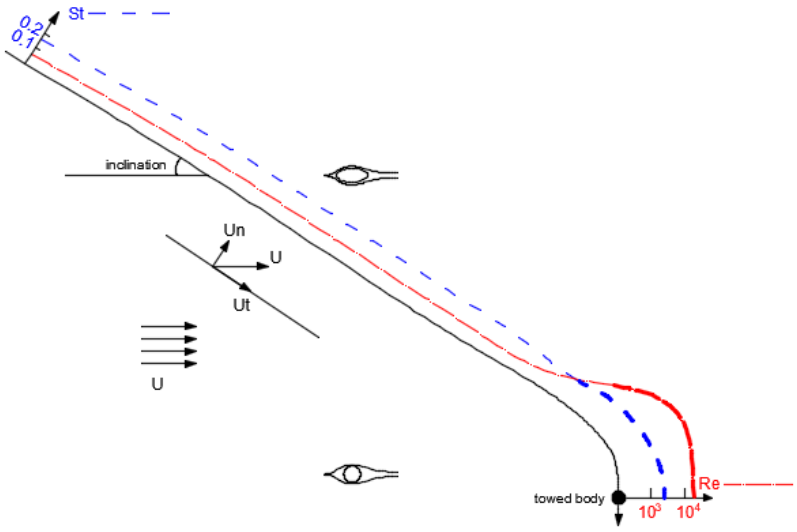

Fig. 6 Re and St distributions along cable profile

model. These detailed towing parameters can be found in Table 2. Towed cable profile in these experimental cases is also given for our coupled scale effect validation.

The distribution of St and ReD along cable is given in Fig. 6. the local flow velocity along cable can be decomposed into axial component U_t and tangential component U_n. Because of a stable inclination along cable, St and ReD are approximate constant in a flow region around an ellipse in horizontal plane. The flow pattern can be considered as flow around a cylinder near towed body.

Table 3 Case setting with different cable diameter scale ratios

cable shape scale ratios (λ)	6	6	6	6	6	6
cable diameter scale ratios (λ_G)	6	4	3	2	1.5	1
scaled cable diameter	0.0017	0.0025	0.0033	0.005	0.0067	0.01
Re_D	3058	4497	5936	8994	12052	17989
flow condition	Laminar flow				Transition to turbulence flow	

The towed cable system with a combination of scaled CFD models is simulated according to this FSI scheme. The integration effect of λ and λ_G.

From Fig. 7, it can be observed that scale ratio of the cable profile is proportionally scaled while the cable diameter is kept unchanged. Deviations in the cable profile occurs due to the same Re is observed in a large λ, while the influence of St effect is neglected.

A cable dynamic prediction agreed better with experimental profile with a constant λ_G = 1 and different λ. Because of a similarity in flow field around scaled model in CFD module and full-scale flow around cable. A cumulative hydrodynamics on cable model in horizontal two-dimensional elliptical cross-sectional wake and transition to cylinder wake is found independent of λ_G scale effect in comparison of wake types of model scale in Fig. 7. It indicates a relative irrelevance of wake in cable flow along axial direction. However, a large λ_G has an increased wake disparity in Fig. 6. Vortex shedding can be found in many large λ_G scale cases. A cumulative effect is also observed for λ_G scale effect. A two-scale ratio system in cable flow can properly give strict wake similarity. This comparison assists a decision of scaled cable model in construction of a high-efficient FSI method in a larger R_{eL} flow. In these large λ_G simulation where vortex shedding with alternative boundary separations has a significant unsteady hydrodynamic distribution along cable. The St number draws more attention in a two-scale ratio system to decide a suitable λ_G. In a situation of low Re otherwise unsteady effect dominated flow around cable is found in this system. St number has to be kept equal in a scale model. The cable profile is found in Fig.8 a to walk back and forth motion in unsteady flow in a transient data transfer FSI simulation.

In this two-scale factors system, because a small scale indicates a lower computational capability, λ =6 is chosen as a scaled model parameter for simulations in Table 3. Another λ_G is changed from 1 to 6 with different $\mathrm{Re_D}$ from 3×10^3 to 1.8×10^5. It can be anticipated that in laminar or turbulent flow various shear layers shedding can be observed in cable wake especially in a cylinder flow region other than elliptical wake. It is also shown that vortex induced vibration occurs much at a cylinder wake region in a tow cable at proportion near towed body.

In these simulations, A good agreement is always found between FSI scaled models calculated and experimental full-scale cable profiles. The $\mathrm{St} = \frac{\mathrm{D}}{\mathrm{V_0 t_0}}$ is decided not only by V_0 and D but also the share layer separation period t_0. However, a long-term time averaged hydrodynamic treatment of scaled model is applied to eliminate this unsteady vortex induced vibration excitation on cable. So, a time-averaged cable profile is presented for validation in Figs. 9 and 10. The deviations of cable profile prediction from experimental cable configuration can be observed to be more obvious with increasing λ_G in Fig. 9. A small λ_G indicates a large $\mathrm{Re_D}$ and the local flow pattern is very close to actual flow around towed cable.

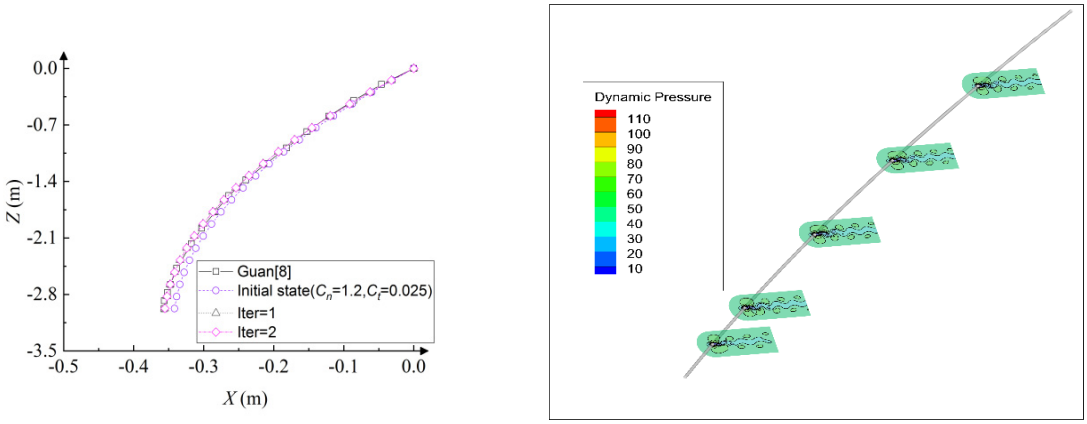

(λ=1, λ_G=1)

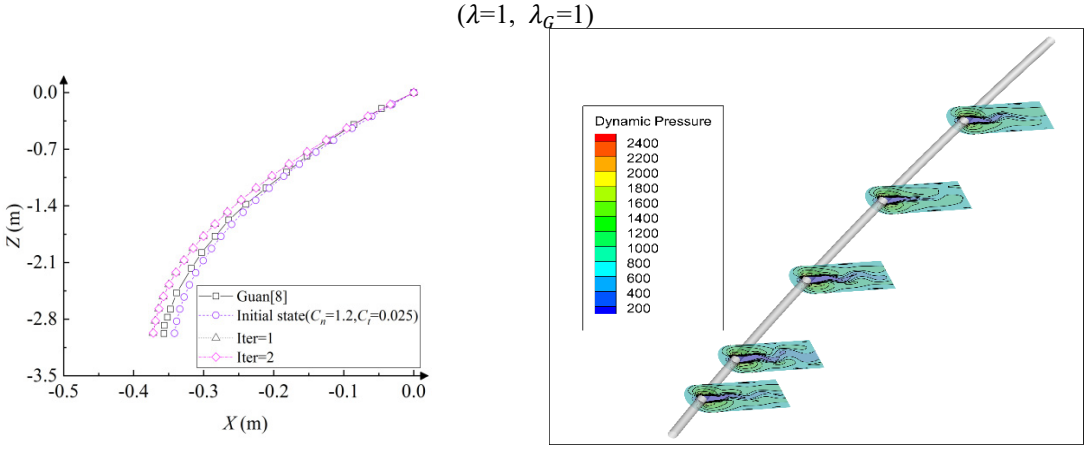

(λ=4, λ_G=1)

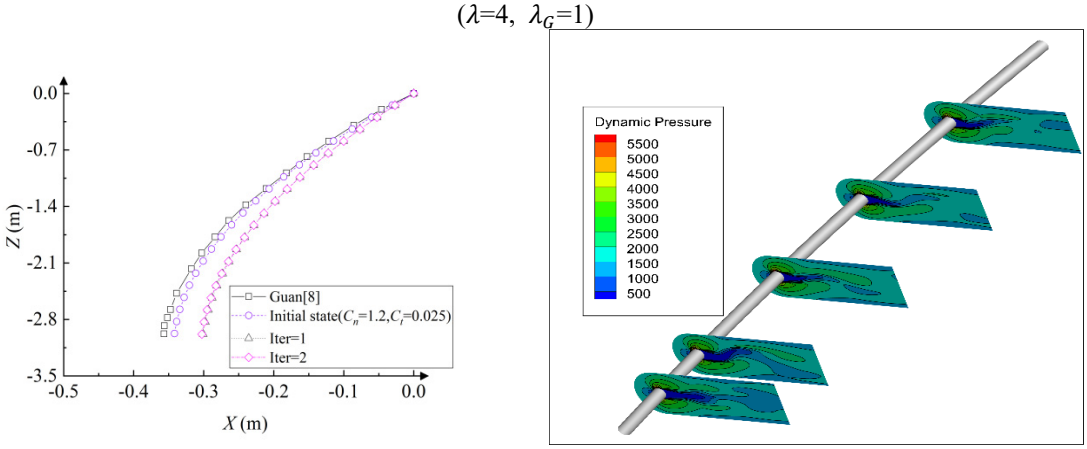

(λ=6, λ_G=1)

Fig. 7 Flow field and dynamic cable profile in a two-scale ratio FSI system with constant Re_D

Time averaged treatment gives a slight spatial fluctuation of vortex drag along with cable profile. These predictions of C_{dx} have an obvious increase with λ_G. This indicates a laminar flow without vortex shedding is in a thick boundary layer and with a higher drag along with decreasing

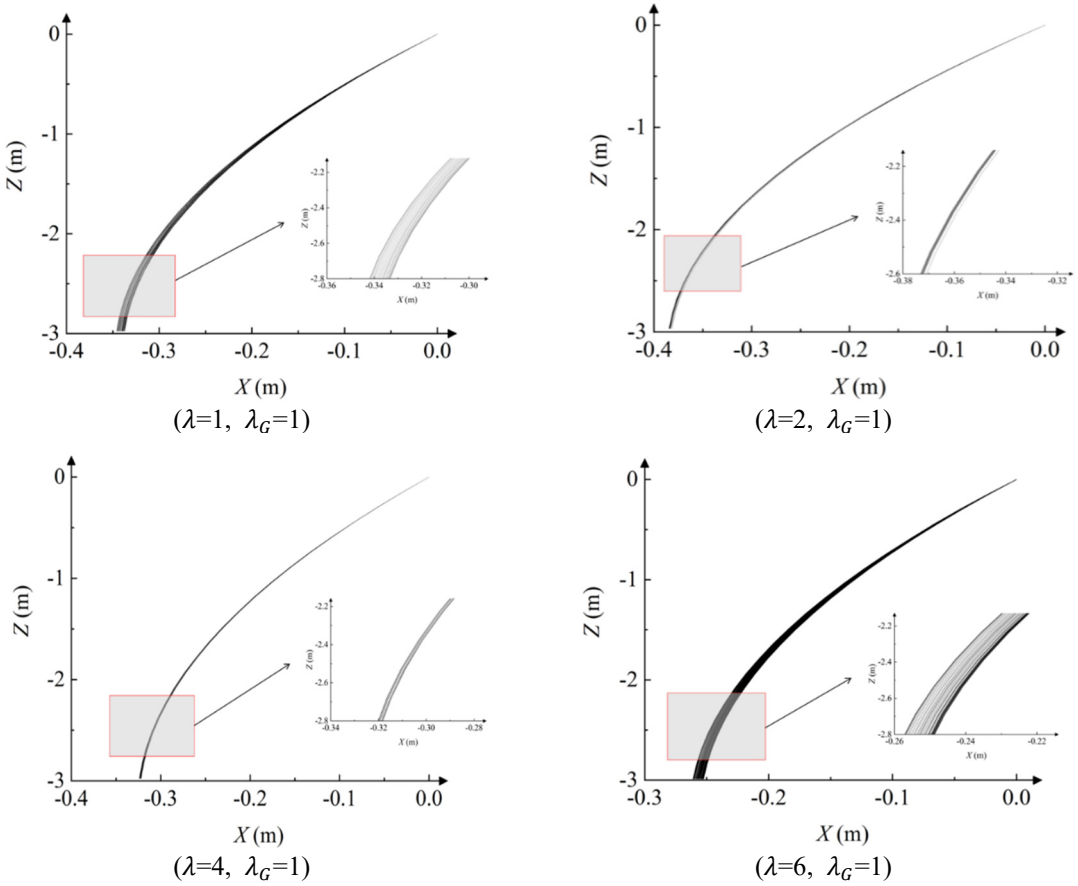

Fig. 8 Vortex induced strumming motions of towed cable in vertical plane

Re_D. Because the towed cable is in a straight tow, C_{dy} can be approximate to zero and C_{dz} is increasing along cable length because of the inclination to flow.

Also, the St number along a cable is changed with flow incidence on cable. In region of flow around ellipse cable section, a low boundary layer separation frequency and a smaller St number is observed. However, in regions of flow around cylinder cable section, the St number is becoming larger according to a high vortex shedding frequency. The critical laminar transition zone to turbulence Re can be 9×10^3 to 3×10^4 in a cylinder wake. In a low Reynolds number tow, laminar cylinder wakes with a significant vortex shedding can be found in far field of a cable flow. It can be a laminar or turbulent vortex. That leads an adjustment in computational domain to obtain a relative stable solution in a scaled model.

There is a further insight into a large vortex structure in a cable flow wake in Fig. 11. The characteristic of a vorticity distribution shows a similarity of vortex shedding between different model scale to ensure FIS simulation accuracy. This is an analogue by two-scale ratios driven model to postulate and maintain a stable spatial vortex structure in an optimal less computational system. There is a significant vortex shedding behavior along cable. It indicates a higher mesh resolution and suitable RANS model.

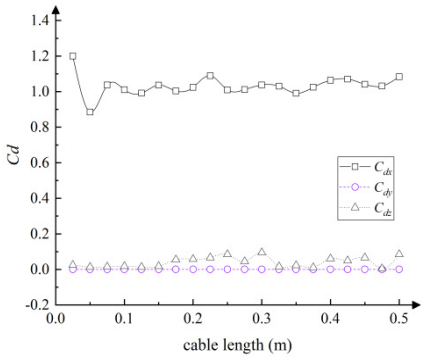

(λ=6, λ_G=1)

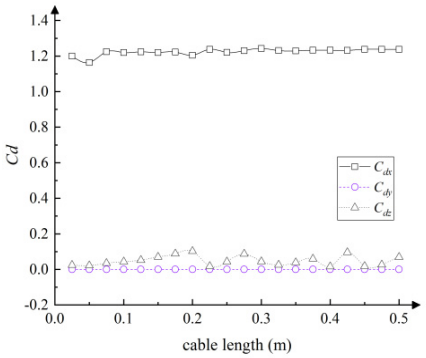

(λ=6, λ_G=1.5)

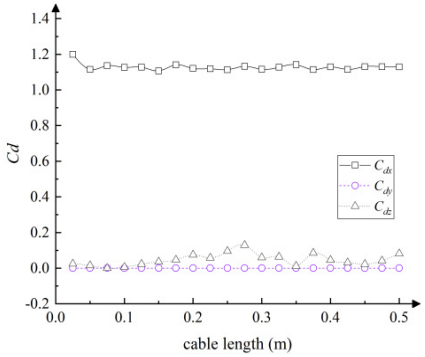

(λ=6, λ_G=2)

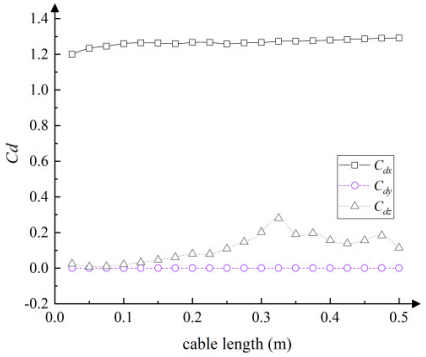

(λ=6, λ_G=3)

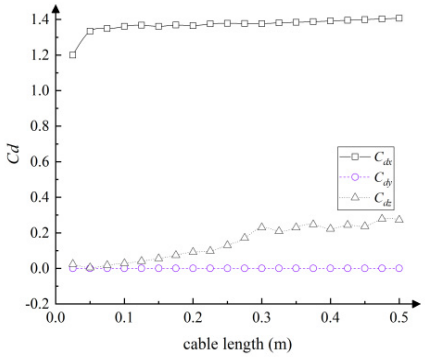

(λ=6, λ_G=4)

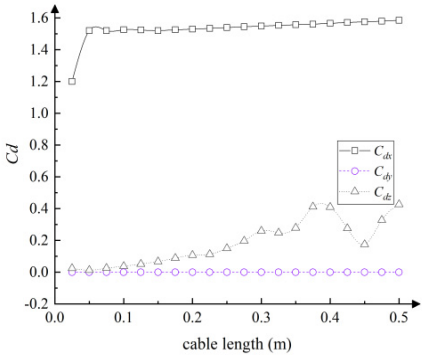

(λ=6, λ_G=6)

Fig. 9 Time-averaged hydrodynamic coefficients along cable of scaled modal

It is illustrated in Fig. 12 the distribution of dynamic pressure on the towed cable profile for different cable diameter scale ratios under the condition of cable shape scale ratio of 6. It is

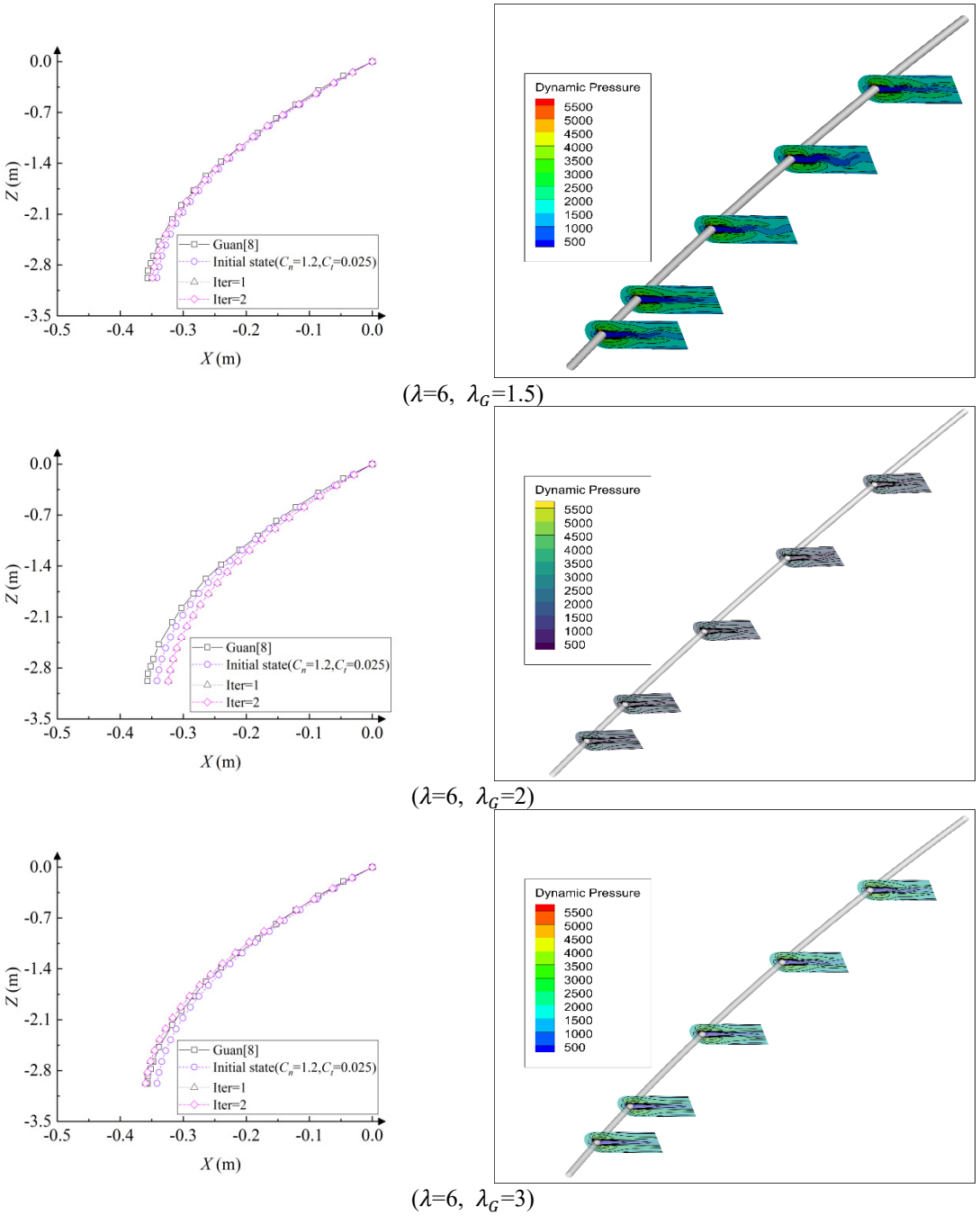

(λ=6, λ_G=1.5)

(λ=6, λ_G=2)

(λ=6, λ_G=3)

Fig. 10 Flow field and dynamic cable profile in a two-scale ratio FSI system with constant Re_L

illustrated as an ellipse flow transition to circular cylinder flow along z cross section. The cross-section flow at z/d=0.9 is used to describe the near towed body separated flow around a cable profile. As the cable diameter scale ratio decreases, the flow field around the cable gradually

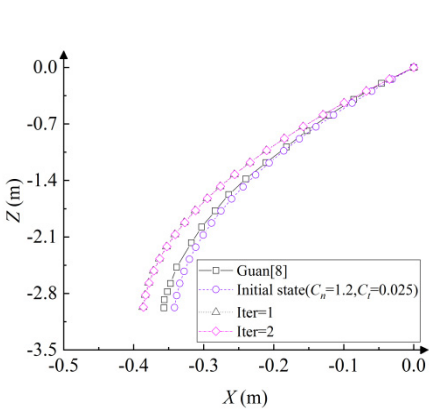

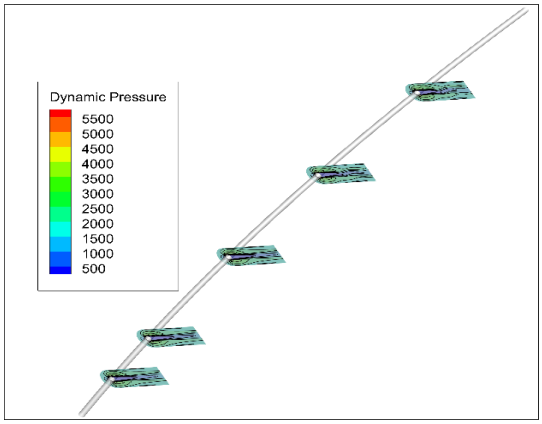

(λ=6, λ_G=4)

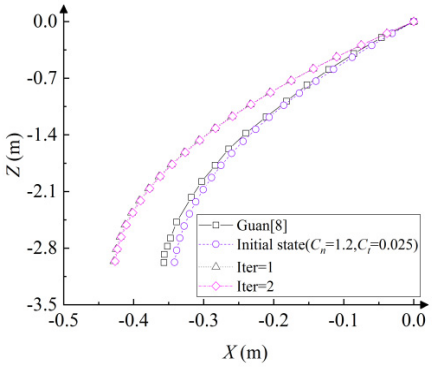

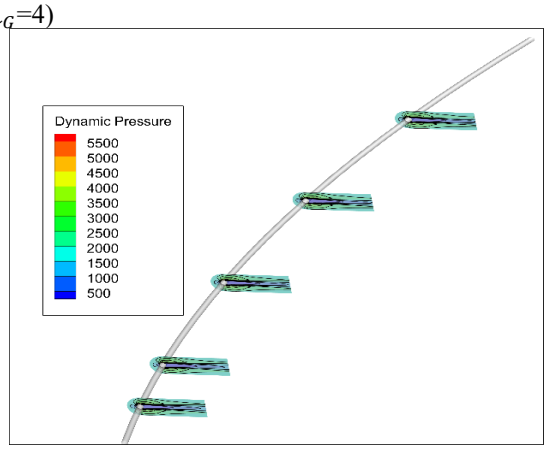

(λ=6, λ_G=6)

Fig. 10 Continued

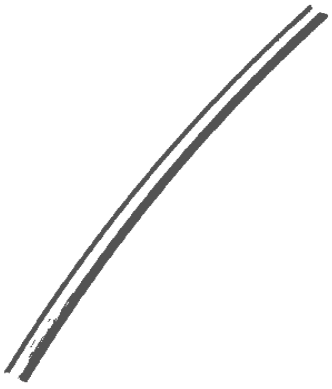

Vorticity= 66 s^{-1} (λ=6, λ_G=6)

Vorticity= 66 s^{-1} (λ=6, λ_G=4)

Fig. 11 Vorticity contour surface in a cable wake

vorticity =46 s^{-1} (λ=6, λ_G=3)

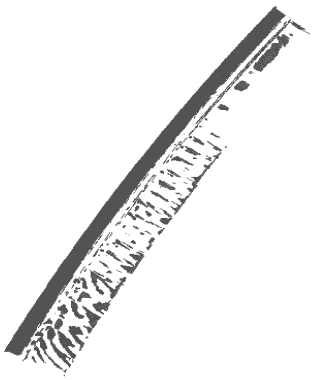

Vorticity = 26 s^{-1} (λ=6, λ_G=2)

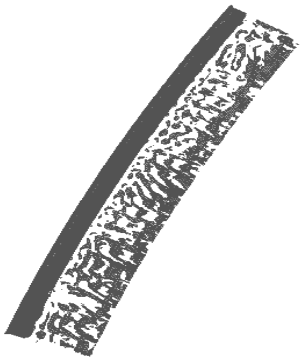

vorticity = 26 s^{-1} (λ=6, λ_G=1.5)

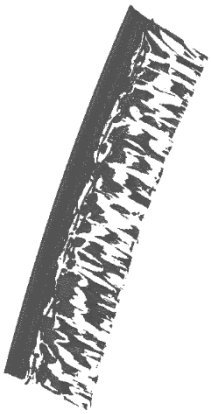

vorticity = 16 s^{-1} (λ=6, λ_G=1)

Fig. 11 Continued-

exhibits alternating shedding of vortices, becoming more similar to the flow pattern around the cable during low tow speed. It indicates a vortex induced cable vibration dominated in a low-speed towing other than snap load from ship motion.

A low turbulent even a laminar flow of a large such as λ_G = 6 can be found with stable symmetrical shear layers in Fig. 9. A high turbulent flow of λ_G = 1 is given for a pair of shear layer alternative shedding into wake. Difference of vortex distributions in Fig. 11 shows a significant scale effect on cable diameter. The two-scale ratios model is very sensitive to λ_G. The vortex generating at certain critical Reynolds number should be carefully investigated based on cable local flow pattern. There is a critical Reynolds number Re_c to determine λ_G in a scaled model. In order to avoid a laminar flow in scaled model, a value of λ_G is necessarily approximate to 1.0 in practices. The λ_G has a determination of laminar or turbulence flow around cable. However, A larger λ can introduce a relatively high velocity and a diminished computational cost.

The Strouhal Number is a dimensionless value useful for analyzing oscillating unsteady fluid flow dynamics problems and interaction with flexible structures. The St number has to satisfy that

$$S_t = \frac{D_0}{U_0 t_0} = \frac{D_1}{U_1 t_1} = \frac{D_1}{\lambda U_0 t_1} \tag{17}$$

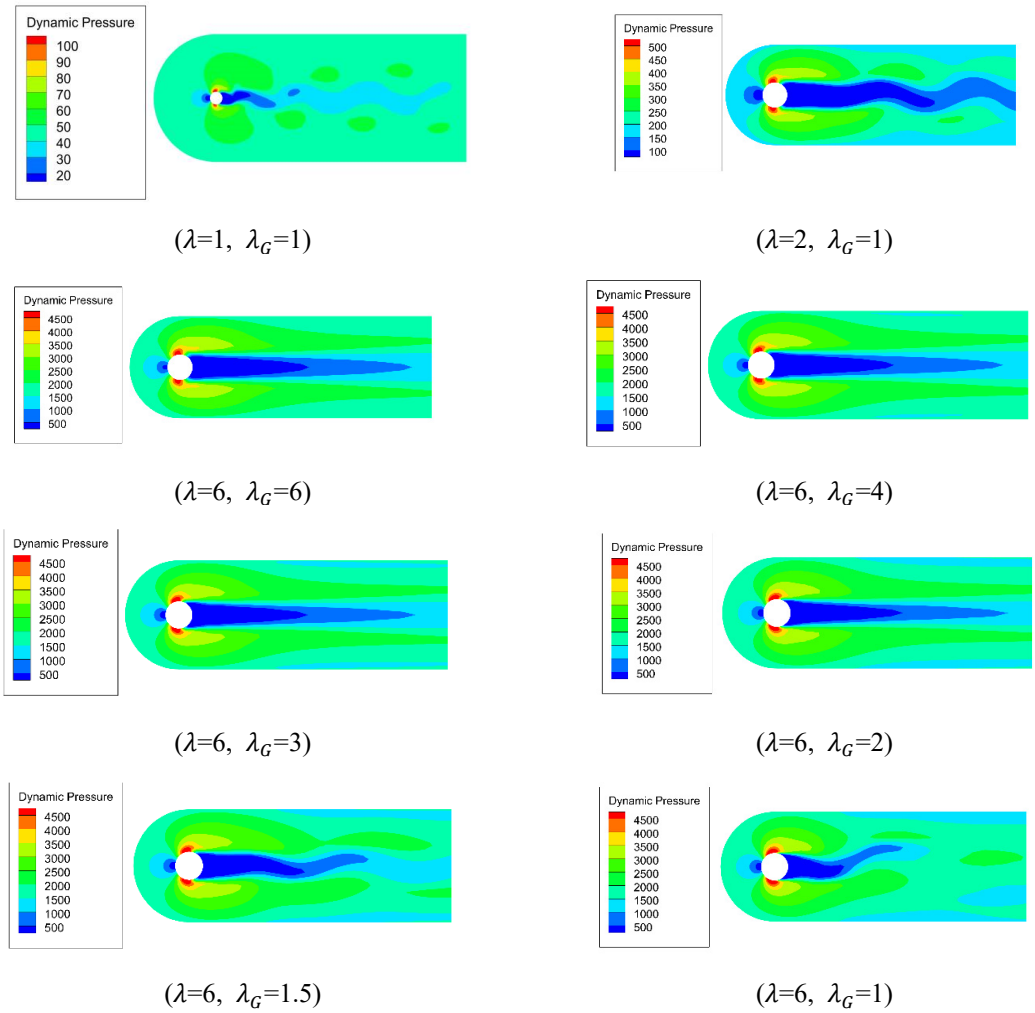

(λ=1, λ_G=1) (λ=2, λ_G=1)

(λ=6, λ_G=6) (λ=6, λ_G=4)

(λ=6, λ_G=3) (λ=6, λ_G=2)

(λ=6, λ_G=1.5) (λ=6, λ_G=1)

Fig. 12 near towed body (z/d=0.9) flow around a cable profile

In which subscript 0 indicates full scale cable, subscript 1 indicates scaled cable model. In order to obtain the unsteady hydrodynamic fundamental frequency of flow around a cable. The total drag history on cable in full scale and reduced scale is given From Figs. 13 to Fig. 16. In comparison of drag frequency in these models of different flow regions the vortex shedding frequency becomes higher with an increasing λ. The St number is becoming stable because of fully developed turbulence flow in a higher Re_D.

3.3 Limit of reynolds number criterion

Another towed cable system from Gobat (1998) is simulated using FSI scheme under two-scale ratios model method. The parameters of this towed system are shown in Table 4. In order to keep a turbulent flow around towed cable, the sensitive parameter $\lambda_G = 1\sim2$ is applied in scaled model.

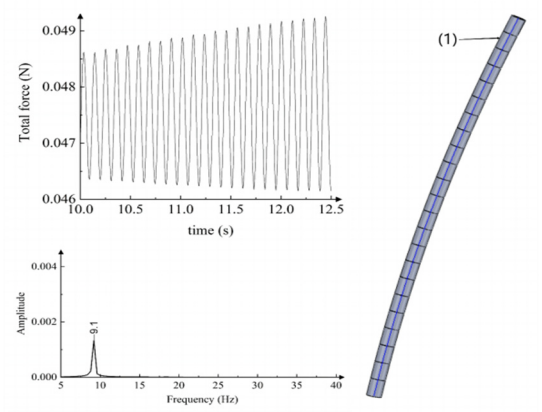

drag force history in cylinder flow region at position (1) $\mathrm{St} = 0.302$

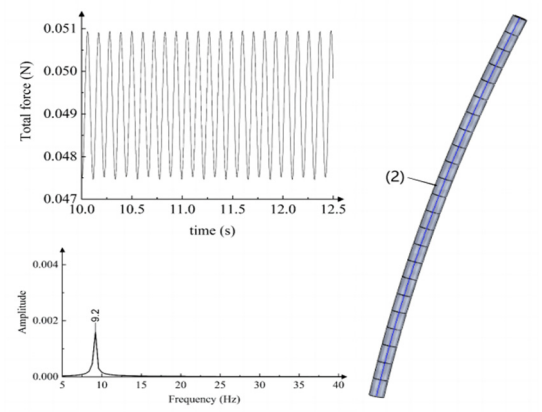

drag force history in cylinder flow region at position (2) $\mathrm{St} = 0.306$

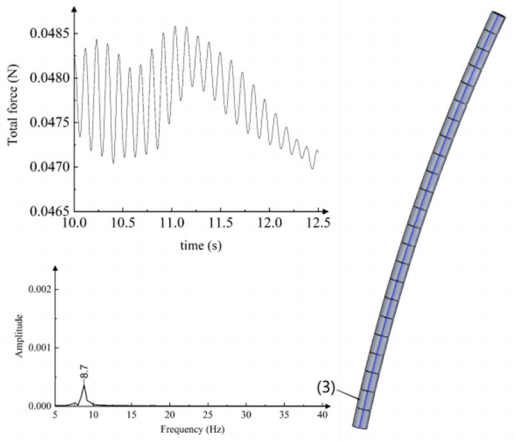

drag force history in cylinder flow region at position (3)

Fig. 13 Total drag force history on different cable segment (λ=1, λ_G=1)

Table 4 Parameters of towed system from Gobat (1998)

Physical parameters of towed cable		Physical parameters of towed body	
Length	L=1000 m	Mass	m=1135 kg
Diameter	D=0.0173 m	Drainage volume of towed body	0.442 m^3
Weight of per unit length	μ=0.00112 kg/m	Drag coefficient	C_{dx}=0.77, C_{dy}=0, C_{dz}=0
Bending stiffness	237.88 kN·m^2	Buoyancy	4448 N
Poisson ratio	0.24	Towed speeds	2.572 m/s
Axial stiffness	12717 kN	Initial C_n	1.5
Torsional stiffness	10 kN·m^2	Initial C_t	0.01

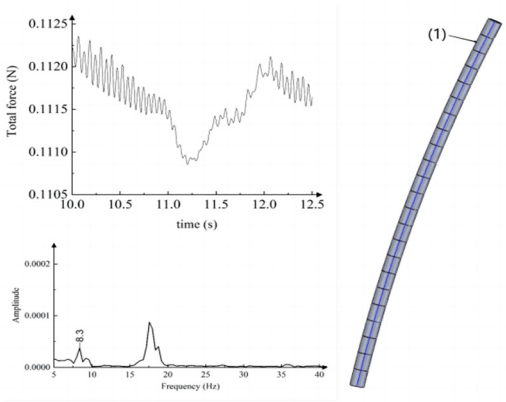

drag force history in cylinder flow region at position (1) $\mathrm{St} = 0.138$

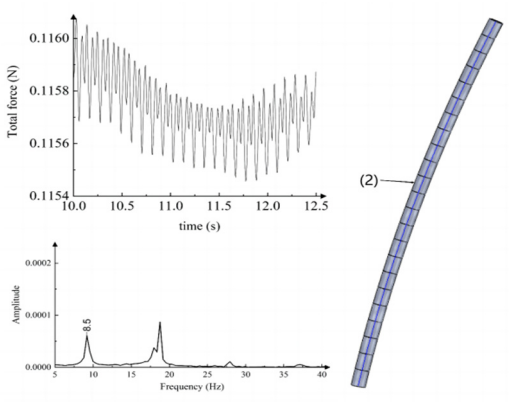

drag force history in cylinder flow region at position (2) $\mathrm{St} = 0.151$

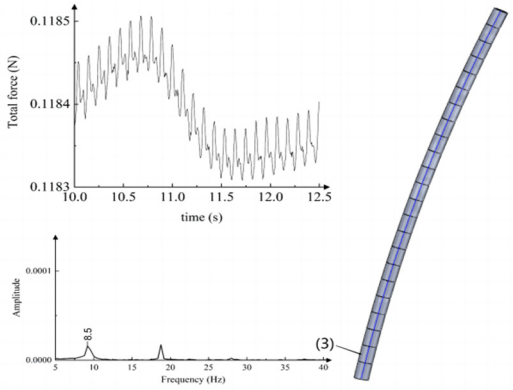

drag force history in cylinder flow region at position (3) $\mathrm{St} = 0.142$

Fig. 14 Total drag force history on different cable segment (λ=2, λ_G=1)

Table 5 Scaled towed cable system

case	cable profile scale ratios (λ), Re
1	50, $Re_U \downarrow$= 266813
2	20, $Re_U \downarrow$=266813
3	12, $Re_U \downarrow$=266813
4	6 , Re =177875
5	4 , Re =148229
6	2 , Re =80852

A range of cable profile scale ratios of λ are used to modelling flow around cable in Table 5. Aimed to obtain a low computational cost in FSI scheme, the Reynolds number is preset to be limited to an estimated upper bound $\mathrm{Re_U}$. The cable is scaled without following the procedure of equal Reynolds number criterion. The cable profile scale ratio λ is between 2 and 50 as in Table 6.

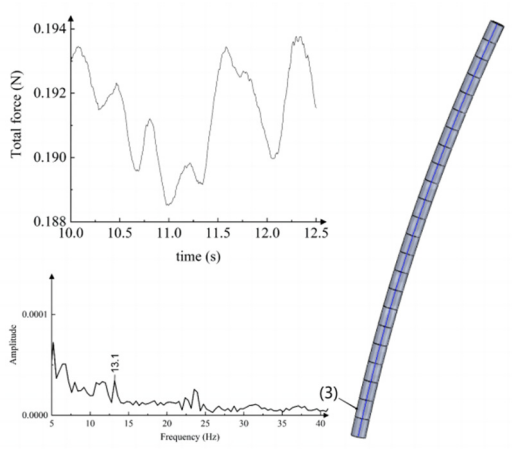

drag force history in cylinder flow region at position (3) $\mathrm{St} = 0.109$

Fig. 15 Total drag force history on different cable segment (λ=4, λ_G=1)

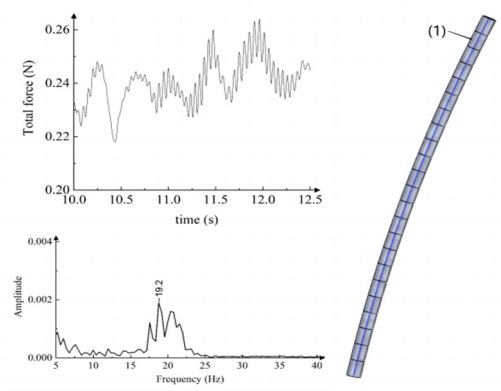

drag force history in cylinder flow region at position (1) $\mathrm{St} = 0.106$

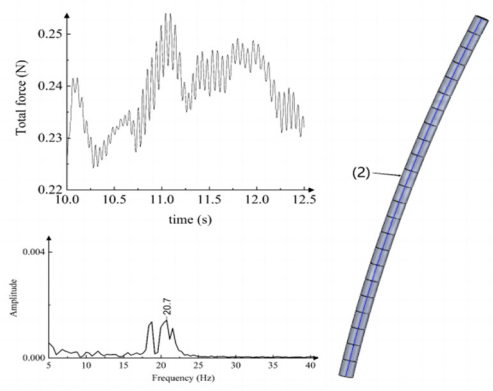

drag force history in cylinder flow region at position (2) $\mathrm{St} = 0.122$

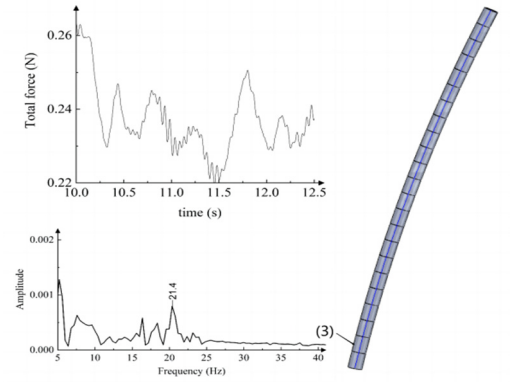

drag force history in cylinder flow region at position (3) $\mathrm{St} = 0.161$

Fig. 16 Total drag force history on different cable segment (λ=6, λ_G=1)

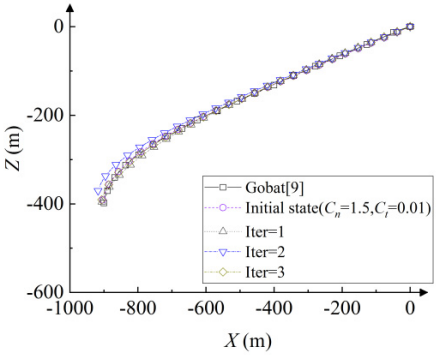

(λ=2, λ_G=1.1)

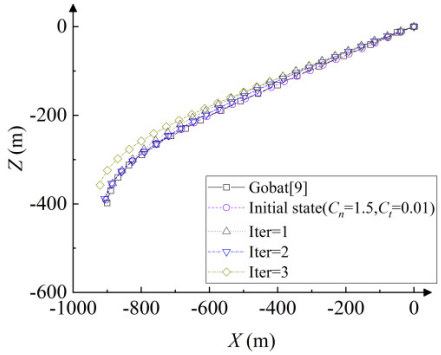

(λ=4, λ_G=1.2)

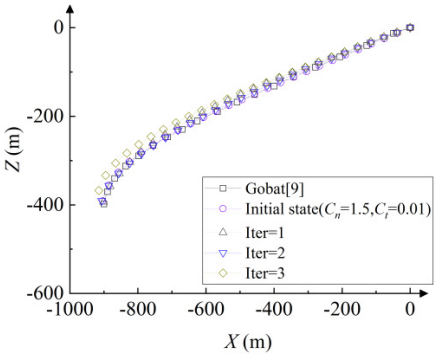

(λ=6, λ_G=1.5)

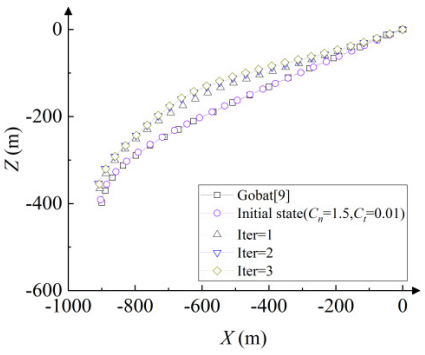

(λ=12, λ_G=1)

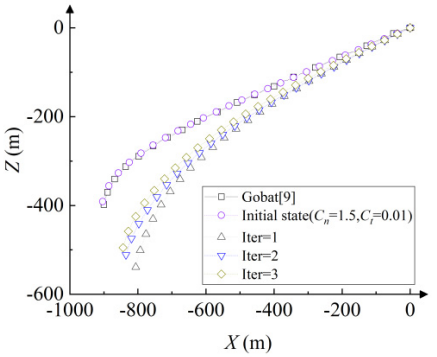

(λ=20, λ_G=1)

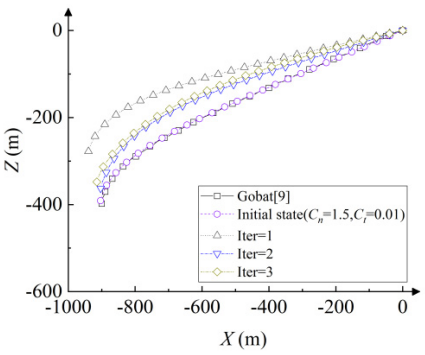

(λ=50, λ_G=1)

Fig. 17 FSI simulation of cable profile in tow-scaled ratio models

This modelling treatment can lower the level of difficulty in generation of boundary layer mesh near cable and numerical false convergence. And, their accuracy depends less on the number of cells describing as few features as possible. Re_U brings an efficient simulation strategy in FSI system.

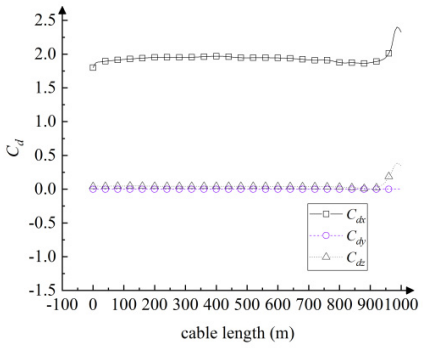

(λ=2, λ_G=1.1)

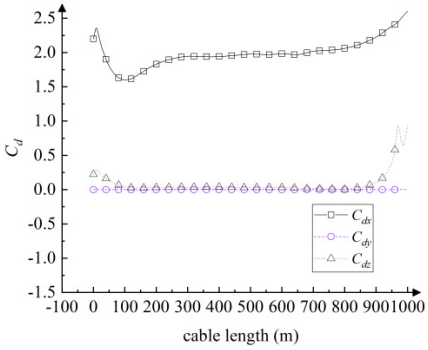

(λ=4, λ_G=1.2)

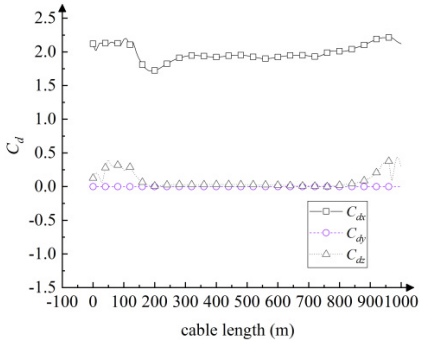

(λ=6, λ_G=1.5)

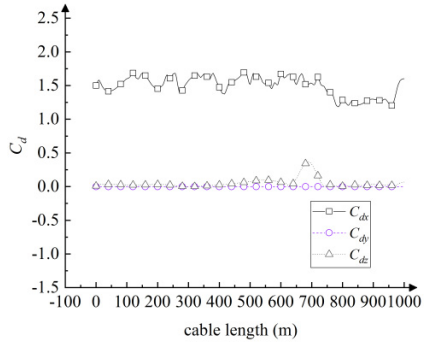

(λ=12, λ_G=1)

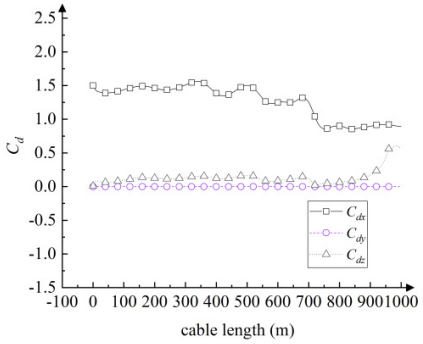

(λ=20, λ_G=1)

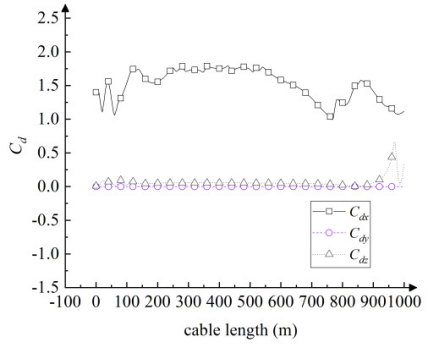

(λ=50, λ_G=1)

Fig. 17 FSI simulation of cable profile in tow-scaled ratio models

In comparison of Fig. 17, a cable profile deviation can be found with an increasing of λ.Because in Fig. 18 the hydrodynamic coefficients are from 2.2 falling into 1.5 with a higher Re. The scale effect can be observed in a bounded Reynolds effect. It can be concluded that coupled effect of λ and λ_G is not obvious in a parameter sensitivity analysis in this model. The wake

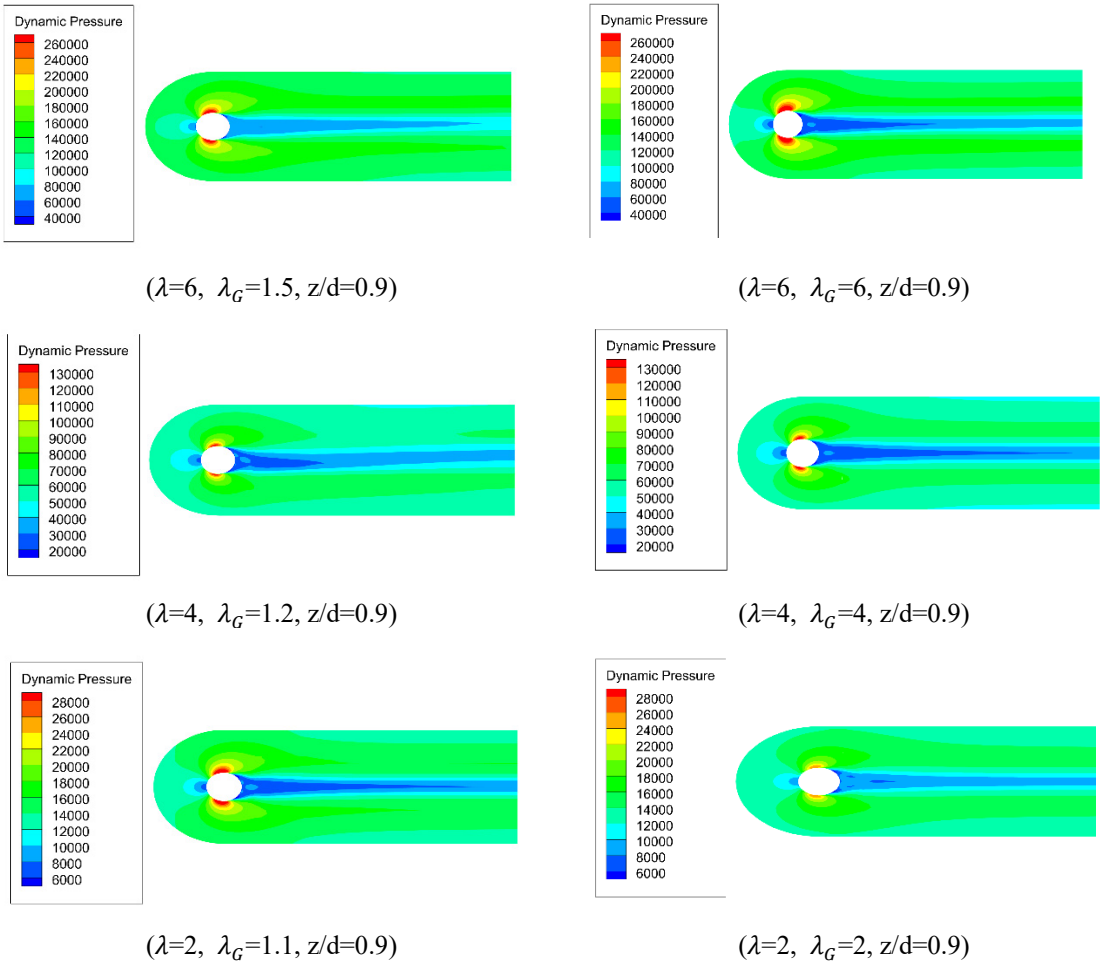

(λ=6, λ_G=1.5, z/d=0.9) (λ=6, λ_G=6, z/d=0.9)

(λ=4, λ_G=1.2, z/d=0.9) (λ=4, λ_G=4, z/d=0.9)

(λ=2, λ_G=1.1, z/d=0.9) (λ=2, λ_G=2, z/d=0.9)

Fig. 19 Towed cable wake structure analysis

types of Fig. 19 become the same pattern in these high λ models. It indicates a high turbulent stable with two shear layers separations.

The upper bound Reynolds number is better chosen as a relatively small value such as $\lambda \leq 6$.

4. Conclusions

This paper introduces an approach of scaled model in a towed cable system. Multiple sets of cases were simulated and calculated using a fluid-structure coupling method. Ensuring the similarity of two flow fields is achieved by maintaining the equality of Re and St before and after scaling. Re plays a primary effect in a scaled cable configuration, while St decides the scaled flow around cable. The conclusions are drawn as follows:

1) Lumped mass method coupled with RANS is innovatively established. This FSI scheme use a normalization interpolation of the scaled cable and prototype.

2) A two-scale ratios cable model system is effectively and efficiently validated based on this FSI method. and Re and St scale effect in this two-scale ratio cable model are fully discussed. Limit of Reynolds number criterion is introduced to reduce computational cost and maintain better performance of FSI system.

3) Effectively reducing the computational scale, for a long towed cable, an appropriate scaling ration procedure can be chosen based on Re and St for the computation. St denotes the relative significance of unsteady effects.

References

Delen, C. and Bal, S. (2019), "Telfer's geosim method revisited by CFD", *Int. J. Mar. Eng*., **161**, 467-478. https://doi.org/10.3940/rina.ijme.2019.a4.563.

Dogrul, A., Song, S. and Demirel, Y.K. (2020), "Scale effect on ship resistance components and form factor", *Ocean Eng*., **209**, 107428. https://doi.org/10.1016/j.oceaneng.2020.107428.

Dong, X., Li, W., Yang, C. and Sun, S. (2018), "RANSE-based simulation and analysis of scale effects on open-water performance of the PPTC-II benchmark propeller", *J. Ocean Eng. Sci*., **3**(3), 186-204. https://doi.org/10.1016/j.joes.2018.05.001.

Farkas, A., Degiuli, N. and Martić, I. (2018), "Assessment of hydrodynamic characteristics of a full-scale ship at different draughts", *Ocean Eng*., **156**, 135-152. https://doi.org/10.1016/j.oceaneng.2018.03.002.

Geuzaine, C. and Remacle, J.F. (2009), "Gmsh: A three-dimensional finite element mesh generator with built-in pre- and post-processing facilities", *Int. J. Numer. Method. Eng*., **79**(11), 1309-1331. https://doi.org/10.1002/nme.2579.

Gobat, J.I. (1998), "WHOI cable: Time domain numerical simulation of moored and towed oceanographic systems", Proceedings of the Oceans.

Guan, G., Zhang, X., Wang, Y., Ji, Z. and Wang, C. (2021), "Analytical and numerical study on underwater towing cable dynamics under different flow velocities based on experimental corrections", *Appl. Ocean Res*., **114**, 102768. https://doi.org/10.1016/j.apor.2021.102768.

Haza, Z.F., Harahap, I.S.H. and Dakssa, L.M. (2013), "Experimental studies of the flow-front and drag forces exerted by subaqueous mudflow on inclined base", *Nat. Hazards*, **68**, 587-611. https://doi.org/10.1109/OCEANS.1998.726374.

Ji, G., Liu, X., Yin, X. and Wang, C. (2021), "Analysis on influence of scale effect on the fluid field at inlet and outlet and thrust of water jet propulsion", *Ship Sci. Technol*., **43**(11), 53-56.

Krasilnikov, V., Sun, J. and Halse, K. (2009), "CFD investigation in scale effect on propellers with different magnitude of skew in turbulent flow", *Proceedings of the 1st International Symposium on Marine Propulsors*, Trondheim, June.

Li, C., Wang, D. and Liu, J. (2020), "Numerical analysis and experimental study on the scaled model of a container ship lashing bridge", *Ocean Eng*., **201**, 107095. https://doi.org/10.1016/j.oceaneng.2020.107095.

Li, D., Berchiche, N. and Janson, C. (2006), "Influence of turbulence models on the prediction of full-scale propeller open water characteristics with RANS methods", *Proceedings of the 26th Symposium on Naval Hydrodynamics*, Rome, September.

Muller, S., Maksoud, M. and Hilbert, G. (2009), "Scale effects on propellers for large container vessels", *Proceedings of the 1st International Symposium on Marine Propulsors*, Trondheim, June.

Neuberger, A., Peles, S. and Rittel, D. (2007), "Scaling the response of circular plates subjected to large and close-range spherical explosions. Part I: Air-blast loading", *Int. J. Impact Eng*., **34**(5), 859-873. https://doi.org/10.1016/j.ijimpeng.2006.04.001.

Oshiro, R.E., Calle, M.A.G., Mazzariol, L.M. and Alves, M. (2017), "Experimental study of collision in scaled naval structures", *Int. J Impact Eng*., **110**, 149-161. https://doi.org/10.1016/j.ijimpeng.2017.01.024.

Pazwash, H. and Robertson, J.M. (1975), "Forces on bodies in Bingham fluids", *J. Hydraul. Res*., **13**(1), 35-55.

Perez-Gruszkiewicz, S.E. (2012), "Reducing underwater-slide impact forces on pipelines by streamlining", *J. Waterw. Port, Coast. Ocean Eng*., **138**, 142-148.

Sanchez, C. (2003), "Simulation of incompressible viscous flow around a tractor thruster in model and full scale", *Proceedings of the 8th International Conference on Numerical Ship Hydrodynamics*, Busan, September.

Sezen, S., Delen, C., Dogrul, A. and Atlar, M. (2021), "An investigation of scale effects on the self-propulsion characteristics of a submarine[", *Appl. Ocean Res*., **113**, 102728. https://doi.org/10.1016/j.apor.2021.102728.

Stanier, M. (1998), "The application of RANS code to investigate propeller scale effects", *Proceedings of the 22nd Symposium on Naval Hydrodynamics*, Washington D.C., August.

Sun, S., Wang, C., Guo, C. and Song, X. (2020), "Numerical study of scale effect on the wake dynamics of a propeller", *Ocean Eng*., **196**, 106810. https://doi.org/10.1016/j.oceaneng.2019.106810.

Terziev, M., Tezdogan, T. and Incecik, A. (2019), "A geosim analysis of ship resistance decomposition and scale effects with the aid of CFD", *Appl. Ocean Res*., **92**, 101930. https://doi.org/10.1016/j.apor.2019.101930.

Wang, F., Dai, Z., Nakahara, Y. and Sonoyama, T. (2018), "Experimental study on impact behavior of submarine landslides on undersea communication cables", *Ocean Eng*., **148**, 530-537. https://doi.org/10.1016/j.oceaneng.2017.11.050.

Wang, F., Tu, W., Deng, D., Wang, Y. and Wang, C. (2019), "Dynamic effect research of cable-lead-in rod on towed system", *J. Shanghai Jiaotong Univ*., **24**, 745-753. https://doi.org/10.1007/s12204-019-2135-x.

Wang, Y. and Wang, W. (2019), "Scale effect analysis on the load difference between inside and outside propeller of four-screw ship", *Ship Sci. Technol*., **41**(23), 11-15.

Wang, Z., Xiong, Y., Wang, R. and Wang, C. (2016), "Numerical investigation of the scale effect of hydrodynamic performance of the hybrid CRP pod propulsion system", *Appl. Ocean Res*., **54**, 26-38. https://doi.org/10.1016/j.apor.2015.10.006.

Windt, C., Davidson, J. and Ringwood, J.V. (2021), "Numerical analysis of the hydrodynamic scaling effects for the Wavestar wave energy converter", *J. Fluids Struct*., **105**, 103328. https://doi.org/10.1016/j.jfluidstructs.2021.103328.

Wu, H. (2016), "Study on scale effect and full scale prediction model of crude oil leakage from underwater damaged tank of double hull tanker", Ph.D. Dissertation, Zhejiang Ocean University, Zhejiang.

Xie, L., Wang, J. and Wan, D. (2021), "The effect of scale effect on bow breaking wave is studied based on DDES", *Shipbuilding of China*, **62**(2), 82-96.

Zakeri, A., Høeg, K. and Nadim, F. (2008), "Submarine debris flow impact on pipelines-part I: Experimental investigation", *Coast. Eng*., **55**, 1209-1218. https://doi.org/10.1016/j.coastaleng.2008.06.003.

Zhou, X., Zhou, W., Hu, X. and Wang, C. (2020), "Similarity theory of flow", *Proceedings of the 31st National Symposium on Hydrodynamics*, Xiamen, November.

ML